The Cerebellum (2019) 18:422–432
https://doi.org/10.1007/s12311-019-1010-5

ORIGINAL PAPER

Biallelic Variants in the Nuclear Pore Complex Protein NUP93 Are Associated with Non-progressive Congenital Ataxia

Ginevra Zanni[1] · P. De Magistris[2] · M. Nardella[1] · E. Bellacchio[3] · S. Barresi[3] · A. Sferra[1] · A. Ciolfi[3] · M. Motta[3] · H. Lue[2] · D. Moreno-Andres[2] · M. Tartaglia[3] · E. Bertini[1] · Wolfram Antonin[2]

Published online: 11 February 2019

Abstract

Nuclear pore complexes (NPCs) are the gateways of the nuclear envelope mediating transport between cytoplasm and nucleus. They form huge complexes of 125 MDa in vertebrates and consist of about 30 different nucleoporins present in multiple copies in each complex. Here, we describe pathogenic variants in the nucleoporin 93 (NUP93) associated with an autosomal recessive form of congenital ataxia. Two rare compound heterozygous variants of *NUP93* were identified by whole exome sequencing in two brothers with isolated cerebellar atrophy: one missense variant (p.R537W) results in a protein which does not localize to NPCs and cannot functionally replace the wild type protein, whereas the variant (p.F699L) apparently supports NPC assembly. In addition to its recently described pathological role in steroid-resistant nephrotic syndrome, our work identifies *NUP93* as a candidate gene for non-progressive congenital ataxia.

Keywords Nucleoporin 93 (NUP93) · Non-progressive congenital ataxia (CA) · Nuclear pore complex (NPC) · Steroid-resistant nephrotic syndrome (SRNS) · Whole-exome sequencing (WES)

Introduction

Non-progressive congenital ataxias (CAs) are a clinically and genetically heterogeneous group of disorders characterized by early onset cerebellar ataxia and other signs of cerebellar dysfunction, which do not progress or even show improvement on follow-up [1]. They account for 10% of non-progressive encephalopathies in the pediatric population. Cerebellar atrophy or hypoplasia is generally detected by neuroimaging. Dominant, recessive, and X-linked forms of non-progressive CA have been reported with over 30 genes identified to date (reviewed in [2, 3], Table S3). To find additional genes that cause non-progressive CA, we performed whole exome sequencing in a family with two affected brothers with non-progressive CA associated with cerebellar atrophy. We report here the identification of biallelic variants in the nuclear pore complex (NPC) protein encoding gene nucleoporin 93 (*NUP93*).

NPCs are large multiprotein complexes that form transport gates in the double membrane structure of the nuclear envelope. They restrict the diffusion of macromolecules and mediate the highly efficient directed transport of proteins, nucleic acids, and RNA-protein complexes between the cytoplasm and the nucleoplasm [4]. NPCs consists of about 30 different proteins, nucleoporins (NUPs), which assemble in multiple copies into NPCs forming a structure of 125 MDa in vertebrates (reviewed in [5]). In addition, some nucleoporins are involved in a variety of other cellular processes such as kinetochore organization, cell cycle regulation, DNA repair, and gene expression (reviewed in [6]). The NPC structural scaffold can be viewed as a stack of three rings: the cytoplasmic and nucleoplasmic rings that are formed by the evolutionary conserved NUP107–NUP160-complex and the inner ring,

Electronic supplementary material The online version of this article (https://doi.org/10.1007/s12311-019-1010-5) contains supplementary material, which is available to authorized users.

✉ Ginevra Zanni
ginevra.zanni@opbg.net

✉ Wolfram Antonin
wantonin@ukaachen.de

[1] Department of Neurosciences, Unit of Neuromuscular and Neurodegenerative Disorders, Bambino Gesù Children's Hospital, IRCCS, 00146 Rome, Italy

[2] Institute of Biochemistry and Molecular Cell Biology, Medical School, RWTH Aachen University, 52074 Aachen, Germany

[3] Genetics and Rare Diseases Research Division, Bambino Gesù Children's Hospital, IRCSS, Rome, Italy

which is mainly formed by multiple copies of the NUP93-complex. The central channel of the pore is occupied by nucleoporins with highly repetitive phenylalanine-glycine (FG)-repeats forming a gel-like structure important for the exclusion and transport capabilities of NPCs. The NUP93-complex is composed of NUP93, NUP155, and NUP53 (also known as NUP35) and the two orthologous NUP205 and NUP188 (for review, see [7]). The NUP93-complex occupies a central position in the NPC architecture, serving as a link between the different nucleoporin subcomplexes including the channel nucleoporins NUP62 (also known as nuclear pore glycoprotein p62), NUP58, NUP54, and NUP45 [8, 9] and connecting the NPC to the pore membrane via direct membrane binding of NUP53 and NUP155 and interaction with transmembrane nucleoporins Ndc1 and Pom121 [10–14].

Recently, biallelic variants in *NUP93, NUP205* [15] and in the NUP107–160 complex components *NUP107*, *NUP85*, *NUP133*, and *NUP160* [16–18] have been identified in patients with isolated steroid-resistant nephrotic syndrome (OMIM#616892; OMIM#614352). Mutations in nucleoporins are also emerging as causes of human neurological disorders: pathogenic variants in *NUP107*, a nucleoporin of the cytoplasmic and nucleoplasmic rings have been identified in nephrotic syndrome associated with microcephaly, simplified gyral patterns and underdeveloped frontal lobes (OMIM#616730) [19]. Similarly, pathogenic variants in *NUP133* have been recently associated to Galloway-Mowat syndrome (OMIM#251300) characterized by early onset nephrotic syndrome, microcephaly and brain anomalies [20]. Mutations in *NUP37*, another nucleoporin of the cytoplasmic and nucleoplasmic rings, were found in patients with microcephaly and intellectual disability [16]. Mutations in *NUP62* cause autosomal recessive infantile bilateral striatal necrosis (OMIM#271930) [21] whereas mutations in the WD-repeat nucleoporin *ALADIN* are associated with the AAA-syndrome (OMIM#231550), characterized by adrenal insufficiency, abnormal development of the autonomic nervous system, and late-onset progressive neurological symptoms including cerebellar ataxia, neuropathy, and dementia [22].

Methods

Subjects

A non-consanguineous Italian family including two affected brothers was enrolled in this study (Fig. 1b). In both patients, recessive inheritance history of congenital non-progressive CA associated with delayed motor milestones with normal cognitive development was observed. Genomic DNA was extracted from peripheral EDTA-treated blood using the blood genomic extraction kit (QIAGEN). All the patients underwent a standard neurologic examination conducted by two qualified neurologists.

Exome Sequencing and In Silico Analysis of the Variants

Targeted enrichment was performed using SureSelect All Exon kit V.4 (Agilent) on genomic DNA extracted from circulating leukocytes from the two affected brothers (II = 1, II = 2) and unaffected parents (I = 1, I = 2). Exome sequencing was carried out on a HiSeq 2000 platform (Illumina). For data analysis, we used an in-house implemented pipeline, which mainly takes advantage of the Genome Analysis Toolkit (GATK V.3.6) framework, as previously reported [23–25]. Reads mapping was performed by BWA V.0.7.12 [26] and GATK tools were used for base quality recalibration and variants calling. SNPs and small INDELs were identified by means of the GATK's HaplotypeCaller used in gVCF mode, followed by family level joint genotyping and phasing, according to GATK's latest best practices. Then, high-quality variants were filtered against public databases (dbSNP147 and GnomAD) to retain private and clinically associated variants, annotated variants with unknown frequency or having MAF < 0.1%, and occurring with a frequency < 1% in an in-house database including frequency data from approximately 1000 population-matched whole-exome sequencing (WES). SnpEff toolbox (V.4.3) [27] was used to predict the functional impact of variants, which were filtered to retain only those variants located in exons with an effect on the coding sequence, and splice site regions (variants located from − 3 to + 8 with respect to an exon-intron junction). Moreover, functional annotation of variants was performed using SnpEff and dbNSFP (V.2.9) [28, 29]. The functional impact of variants was analyzed by combined annotation-dependent depletion (CADD) V.1.3, algorithm [30]. WES statistics are reported in Table S1. Variant validation and segregation was performed by Sanger sequencing.

NUP93 Depletion and Add-Back Assays in *Xenopus laevis* Eggs

Nuclear assemblies using *X. laevis* egg extracts, immunofluorescence on in vitro-assembled nuclei and the generation of affinity resins, sperm heads, and floated, unlabeled, or DiIC18 (1,1′-dioctadecyl-3,3,3′,3′-tetramethylindocarbocyanine perchlorate)-labeled membranes were carried out as described [31] and results were analyzed on an Olympus FV1000 confocal microscope. NUP93 was depleted as in [32] by incubating high-speed extracts twice with a 1:1.2 bead to cytosol ratio for 20 min. For rescue experiments, mRNA encoding human NUP93 (GenBank, NM_014669.4) and the corresponding variants was prepared using the mMESSAGE mMACHINE kit (Life Technologies) and added to extracts at a

concentration of 150–200 ng/μl [13]. The experiment was repeated three times independently, and 100 nuclei were counted in each experiment. mAB414 (Covance) was used in immunofluorescence as a general NPC marker. Antibodies against NUP93, NUP62, and NUP58 have been described before [8], MYC antibody (9E10) was obtained from Merck. DiIC18, secondary antibodies (Alexa Fluor 488 goat α-rabbit IgG and Cy3 goat α-mouse IgG) and DAPI (4′,6-diamidino-2-phenylindole, dihydrochloride) were obtained from Invitrogen.

For the experiments combining different NUP93 variants in the in vitro reconstitution assay (Fig. S3), the mRNA encoding human NUP93 and the corresponding variants were translated in 40 μl NUP93-depleted egg extracts in the presence of 1 μl FluoroTect™ GreenLys tRNA or Transcend™ tRNA (Promega) resulting in BODIPY-labeled or lysine-biotinylated NUP93 variants, respectively. After 1 h of incubation at 20 °C, the in vitro translation was stopped by addition of 50 μg/ml cycloheximide. For nuclear assembly two 10-μl samples of the different in vitro translation reactions were combined and processed as described above. Lysine-biotinylated NUP93 variants were detected by addition of 0.1 μg/ml of Alexa Fluor 546-labeled streptavidin to the nuclear assembly reaction 5 min prior to fixation.

Coimmunoprecipitation Assays

For immunoprecipitations, EGFP-NUP93 constructs were transfected into HEK293 cells using jetPRIME (polyplus transfection). Then, 24 h post-transfection cells were harvested and lysed in lysis buffer (50 mM TRIS-HCl pH 7.5, 150 mM NaCl, 1 mM EDTA, 10% glycerol, and 0.1% Triton X-100 supplemented with protease inhibitors (2 μg/ml leupeptin, 1 μg/ml pepstatin, 2 μg/ml aprotinin, 0.1 mg/ml AEBSF final concentration) for 30 min at 4 °C. After centrifugation for 15 min at 15,000×*g*, the supernatant was pre-cleaned by passage over sepharose beads and immunoprecipitated with GFP-Trap beads (Chromotek) for 2 h, washed 5× with lysis buffer, 2× with lysis buffer supplemented with 500 mM NaCl, 2× with lysis buffer, and 1× with lysis buffer without Triton X-100 and finally eluted with SDS-sample buffer. Eluates and lysed cells (corresponding to 5% of the eluates) were analyzed using anti-EGFP antibodies (Roche, 11814460001), NUP205, NUP188, and NUP98 antibodies have been described before [8, 32].

Fibroblast Cell Cultures

Skin biopsy was obtained after informed consent from patient II = 1. Fibroblast were grown in 25-ml culture flasks in DMEM and 10% fetal calf serum. Then, 5–6000 cells from the primary culture were transferred to 35-mm Petri dishes 2 days prior to fusion.

Expression of NUP93 Transcripts in Human Tissues and Fibroblasts

For testing, the expression levels of the NUP93 variants by qPCR total RNA was isolated from 1×10^7 mutated and wild type fibroblasts with QIAGEN RNeasy® Mini Kit according the manufacturer's instruction (Fig. S2A). Reverse transcription of the first-strand cDNA was done using ThermoFisher RevertAid First Strand cDNA Synthesis kit (Cat No./ID: 1621). qPCR was performed using allele specific PCR with a blocking reagent [33]. All primers and probes as well as blockers were obtained from Integrated DNA Technologies (Table S2). Triplex TaqMan PCR was done in a volume of 10 μl with 5 μl PrimeTime® Gene Expression Master Mix (Integrated DNA Technologies), 500 nM primers, 250 nM probe, and 2000 nM blocker. The qPCR was carried out in a QIAGEN RotorGene with TaqMan thermocycling conditions: 10 min at 95 °C, 50 cycles of 15 s at 95 °C, 20 s at 60 °C, and 20 s at 72 °C. All PCR assays were run as triplicates.

Isolation of RNA was performed by QIAGEN RNeasy® Mini Kit (Cat No./ID: 74104) following standard protocol. Expression of NUP93 transcript was analyzed by RT-PCR in human fetal brain, adult brain, and cerebellum (Fig. S2B).

Molecular Modeling

Analysis of the effects of the R537W and F699L variants in NUP93 were made employing the structure of the inner ring of the human nuclear pore complex (Protein Data Bank id 5IJN, 5th model, chain C [34]. Side chains were constructed with SIDEpro [35].

Results

Clinical Evaluation of Patients

The clinical features of the two affected brothers (aged 20 and 23) born to healthy non-consanguineous parents, consisted of developmental delay, neonatal hypotonia, and early onset (within the first years of life) nonprogressive cerebellar symptoms: nystagmus, ataxia, and dysarthria. Head circumference and cognitive development were normal. EEG, metabolic, and renal workup were repeatedly normal. Karyotype and array-SNP analysis were negative. Neuroimaging studies performed at 10 and 13 years of age, respectively, revealed a global cerebellar atrophy with normal cortex and brainstem (Fig. 1a–d).

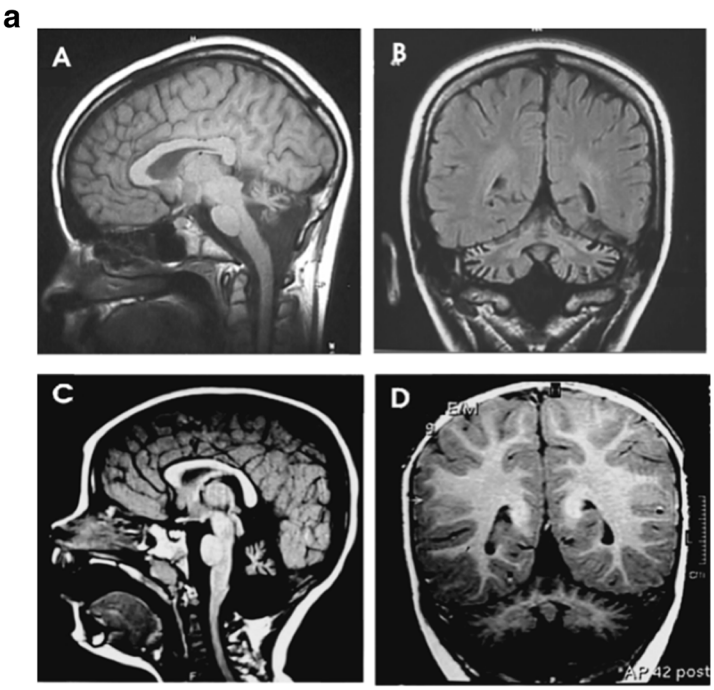
a
A
B
C
D

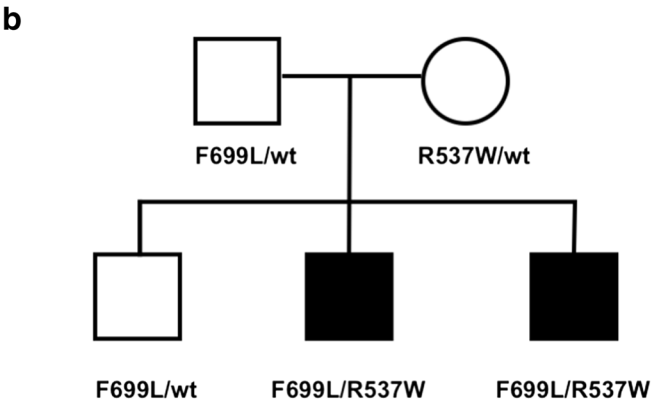
b
F699L/wt
R537W/wt
F699L/wt
F699L/R537W
F699L/R537W

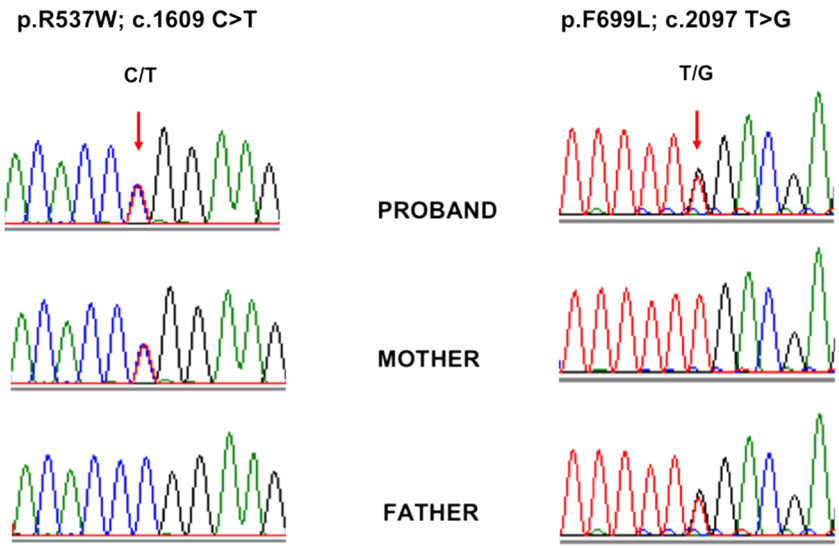
p.R537W; c.1609 C>T
C/T
p.F699L; c.2097 T>G
T/G
PROBAND
MOTHER
FATHER

◀ **Fig. 1** Pedigree structure, electropherograms, and brain MRI studies of *NUP93*-mutated patients. **a** Upper panel = Neuroimaging studies: T1 weighted mid-sagittal section (A, C) and T1 weighted coronal section (B, D) of the mutated patients, showing global cerebellar atrophy without cortical or brainstem involvement. **b** Middle panel = pedigree of the family. Lower panel = chromatograms of the two *NUP93* pathogenic variants

Exome Sequencing and In Silico Analysis of the Variants

Whole exome sequencing identified two rare missense variants in *NUP93* (NM_014669.4:c.1609C > T);(p.R537W); rs371707121 with a frequency of 1.62466e-05 in the GnomAD database whereas the second variant (NM_014669.4:c.2097T>G); (p.F699L) is not reported in genomic databases. The mutated residues of NUP93 are both well conserved across different species (Fig. 2, upper panel). Both pathogenic variants were predicted to be damaging by in silico prediction tools (Polyphen 2, SIFT, and PROVEAN for R537W, SIFT and PROVEAN for F699L). Segregation analysis by Sanger sequencing in the family confirmed autosomal recessive inheritance (Fig. 1b). A third rare missense variant was found in the *ARAF* gene (NM_001654.4:c.1198C>T); (p.R400C); rs754803899. This X-linked variant was inherited from the mother and was the only X-linked gene satisfying the co-segregation criterion. It was excluded as disease causing because a variant affecting the same residue p.R400H (rs764255925) was reported in a male control individual in the Geno2MP database (http://geno2mp.gs.washington.edu). Moreover, the amino acid change in ARAF did not show an impact on protein stability or substrate phosphorylation (Supplementary data).

Localization of NUP93 Variants to NPCs and NPCs Assembly

In order to explore the impact of the two missense variants on NUP93 function, we assessed the subcellular localization and the capability of the NUP93 variants to recruit other nucleoporins and integrate into NPCs. We transfected HeLa cells with EGFP-NUP93 fusion constructs. The wild type version and the F699L variant localized to the nuclear envelope and co-stained with mAB414, an antibody which recognizes NPCs (Fig. 3a). In contrast, the R537W variant showed a nuclear localization but no co-staining with mAB414 at the nuclear envelope. This indicates that this variant does not integrate into NPCs. Next, we checked whether the pathogenic variant affected known NUP93 interactions to other nucleoporins. For this, we transfected HEK293 cells with the different EGFP-NUP93 fusion constructs, generated cellular extracts and performed EGFP-pulldown experiments testing by Western blotting for co-precipitation of other nucleoporins (Fig. 3b). Interaction with NUP188 and NUP205, which bind NUP93 in a mutual exclusive manner [32], was not affected by the NUP93 variants.

NUP93 is found in fibroblasts obtained from patients at the nuclear envelope in a typical NPC staining pattern (Fig. S1A). Western blotting indicated that the protein is indeed present in patient fibroblasts (Fig. S1B). qRT-PCR indicated that in these cells both NUP93 variants are equally expressed summing up to approximately the same levels as in age and sex-matched biallelic wild type control (Fig. S2A).

Interference of NUP93 Variants with Nuclear Envelope Integrity

To further evaluate the interference of the two identified variants with nuclear envelope integrity, we performed a depletion-addback assay in *X. laevis* egg extracts where formation of a functional nuclear envelope including NPCs can be faithfully reconstituted [31, 36]. Importantly, in this in vitro system, also lethal mutations can be individually and conveniently tested [15]. NUP93 can be efficiently depleted using specific antibodies without affecting the levels of other nucleoporins as indicated by the signal for the central channel nucleoporin NUP62 (Fig. 4a). Sperm DNA were incubated in mock-treated extracts, forming a closed nuclear envelope (indicated by the membrane staining Fig. 4b, first row; see Fig. 4c for quantitation) with NPCs (labeled with the antibody mAB414, Fig. 4b, third row). Depletion of NUP93 blocked nuclear envelope and pore formation as previously reported [8, 32, 37]. This phenotype was restored upon addition of mRNA expressing myc-tagged versions of wild type NUP93 (Fig. 4b, third column) which was added in amounts to restore approximately endogenous NUP93 levels (Fig. 4a). In these assays, the myc-tagged F699L variant (Fig. 4b, fifth column) but not the myc-tagged R537W variant (Fig. 4b, fourth column) was able to replace the wild type protein.

NUP93 functions in linking the pore membrane to the central channel nucleoporins [8, 9]. Consistent with this, depletion of NUP93 abolishes staining of NUP58, a component of the NUP62-NUP58-NUP54/45 complex, which forms a large part of this central channel. Interestingly, in contrast to the R537W variant, the F699L variant was able to restore NUP58 staining. Together, these data indicate that the F699L variant is able to function in NPC assembly whereas the R537W variant cannot fulfill this task.

When mRNAs expressing both NUP93 variants, R537W and F699L, were added to NUP93-depleted extracts, only the F699L version was located to NPCs (Supplemental Fig. S3). When co-expressing with wild type NUP93, F699L together with the wild type NUP93 was found at NPCs but not R537W. This supports the hypothesis, that R537W is a functional null mutation whereas the F699L mutation does not prevent NPC assembly.

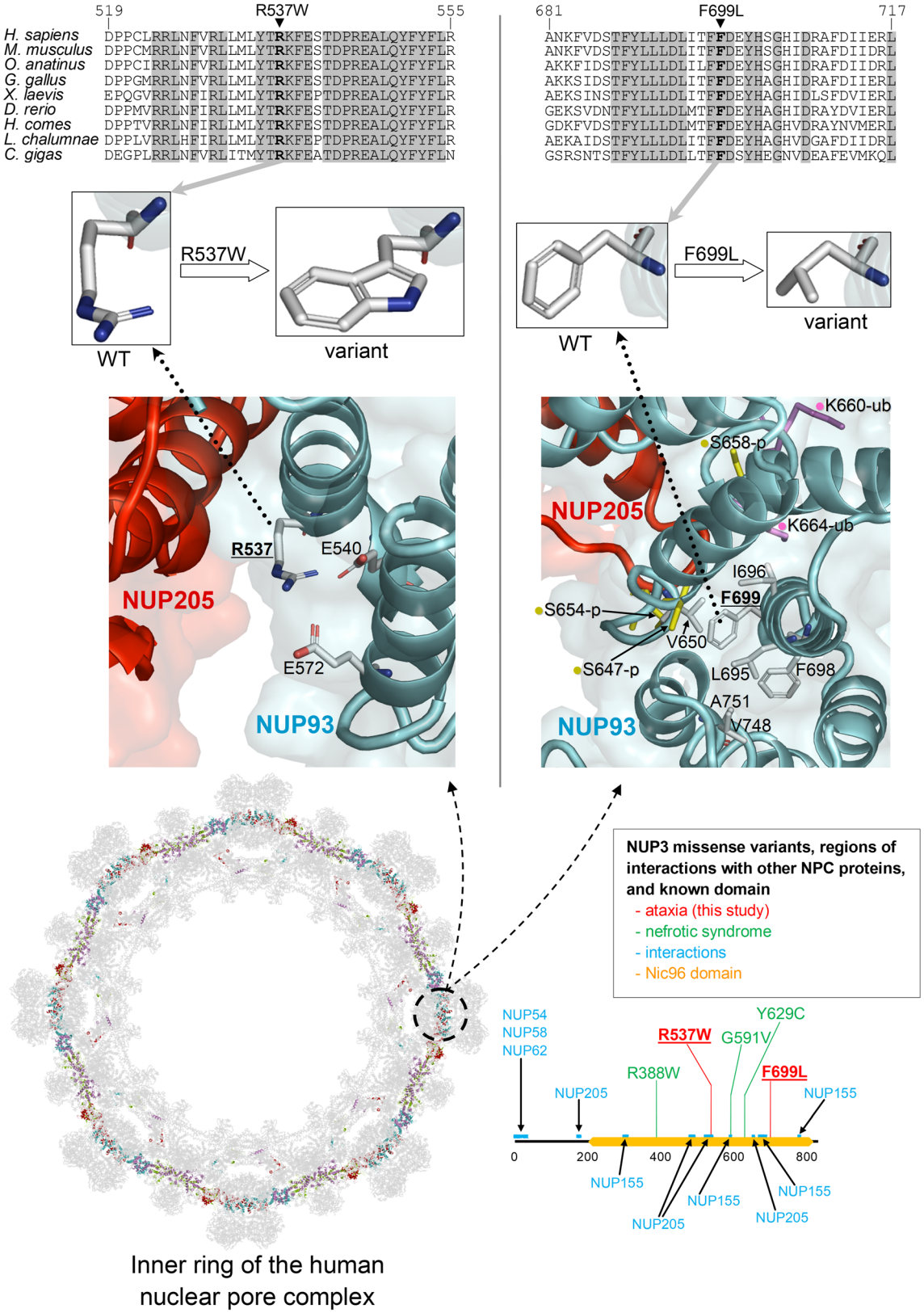

Inner ring of the human nuclear pore complex

◀ **Fig. 2** Molecular 3D modeling of the NUP93 variants. Upper panel = Sequence alignment of NUP93 proteins among species around the sites of the R537W and F699L variants (invariant residues are indicated in gray). Lower panel, left = Structure of the inner ring of the human nuclear pore complex (from PDB structure 5IJN). The distinct NUP93 monomers are represented in different colors, other nuclear pore complex components (NUP155, NUP205, NUP54, NUP58, and the nuclear pore glycoprotein p62, also referred to as NUP62) in gray. Enlarged views of the regions affected by the R573W and F699L variants are shown for the NUP93 monomer encircled by the dashed line (for clarity, in these representations only NUP93, cyan, and NUP205, red, are shown). Lower panel, right = Scheme of the NUP93 protein indicating missense variants and their related phenotypes (the ataxia variants reported in this study are in red, and the previously published nephrotic syndrome variants in azure) and putative interaction regions of NUP93 with neighboring the nuclear pore complex proteins (indicated in the labels), based on the PDB structure 5IJN of the human nuclear pore complex inner ring scaffold

Molecular 3D Modeling

The available structure of the inner ring of the human NPC was used to model the possible structural and functional consequences of the NUP93 variants [34]. The R537W variant affects a highly conserved arginine residue that contributes to the structure of NUP93 by forming salt-bridges with the proximal E540 and E572 residues (Fig. 2, lower panel). The replacement of the cationic arginine with the large and uncharged tryptophan residue thus disrupts these intramolecular binding networks in the model. In addition, as indicated in the detailed view, the R537 residue of the NUP93 monomer is located at the interface of the protein with a NUP205 chain, which leads us to envisage a structural perturbation introduced by the arginine to tryptophan substitution with possible impact on NPC assembly. The F699L change occurs within a cluster of hydrophobic residues and the replacement of phenylalanine with another hydrophobic residue may not generate important structural changes, which is consistent with the collected data indicating the absence of any relevant consequences of the phenylalanine to leucine substitution on NPC assembly and interaction with NUP205. However, the site affected by this variant is surrounded by several residues shown to undergo

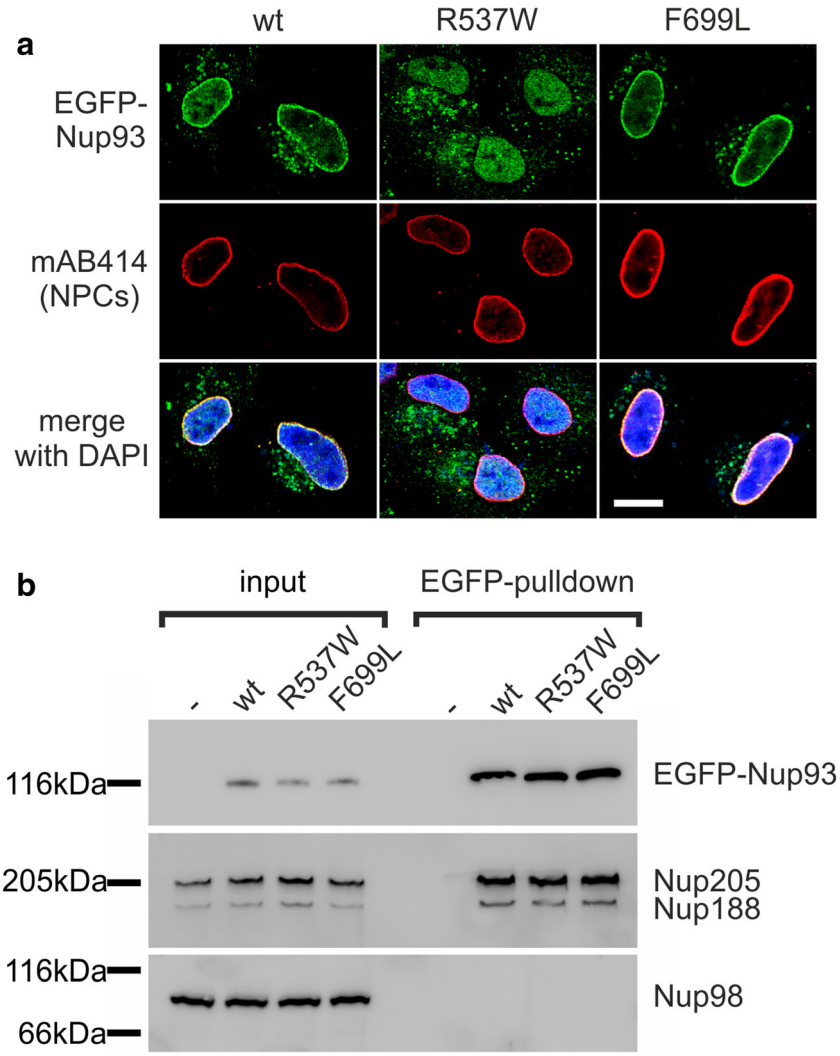

Fig. 3 The NUP93 p.R537W variant interferes with integration into nuclear pore complexes. **a** HeLa cells were transfected with different EGFP-NUP93 fusion constructs, fixed 24 h post transfection and stained with the NPC marker mAB414 (red) and DAPI. The EGFP-NUP93 signal is shown in green. Scale bar 10 μm. **b** HEK297 cells were mock transfected or with indicated EGFP-NUP93 fusion constructs. Immunoprecipitates and 5% of the inputs from cell lysates generated 24 h post-transfection were analyzed by western blotting for the NUP93 interactors NUP188 and NUP205. NUP98 served as a negative control for a non-interacting nucleoporin

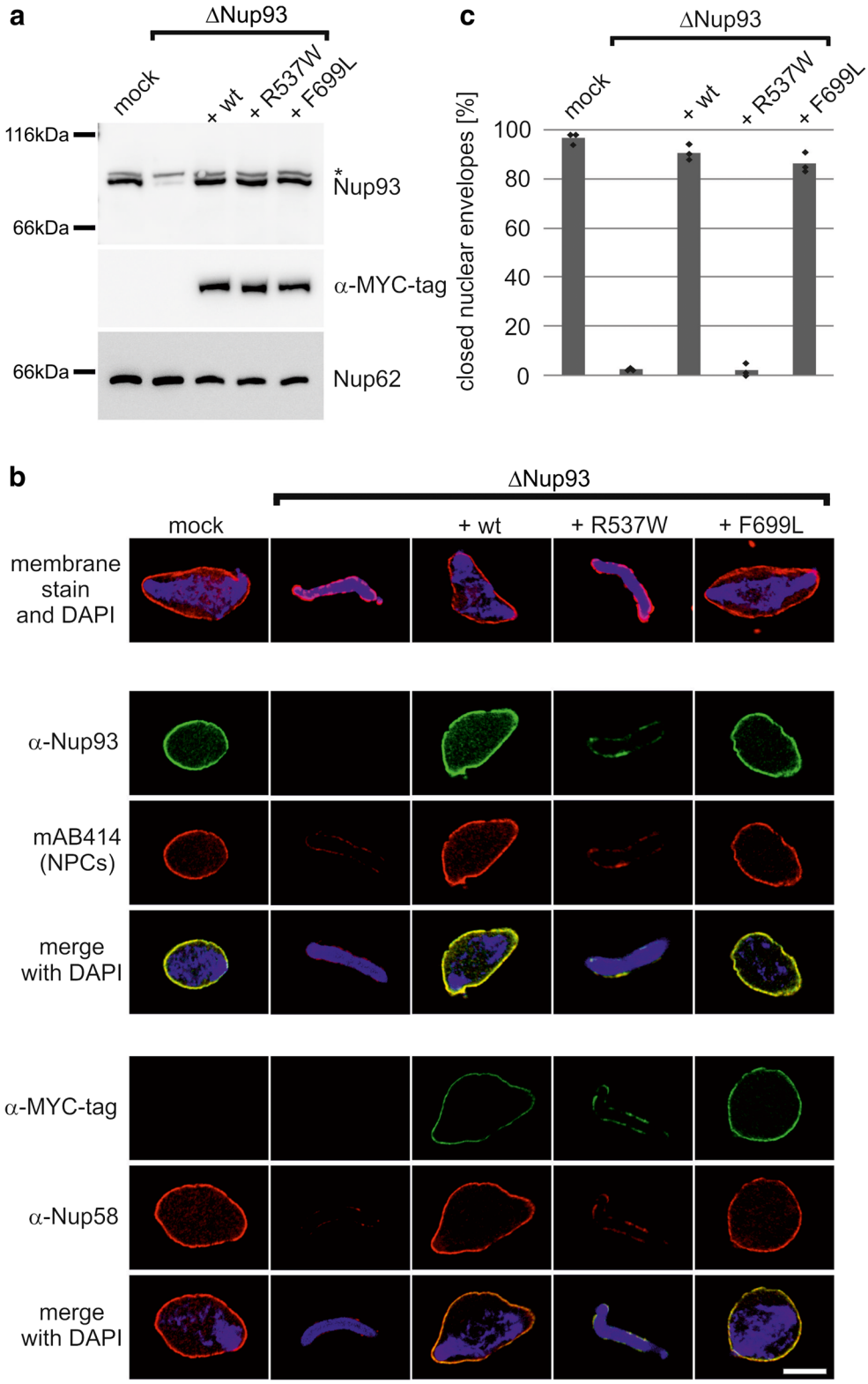

post-translational modifications including phosphorylation of serines: S647, S654, and S658 (yellow sticks, been shown to have an important function in regulating nucleoporin protein-protein interactions [38, 39].

Discussion

NPCs play a crucial role in all nucleated cells mediating the essential transport between cytosol and nuclear interior.

◀ **Fig. 4** The NUP93 p.R537W variant is not functional in NPC assembly. **a** Western blot of mock, NUP93 depleted (ΔNUP93) and NUP93 depleted extracts supplemented with mRNA coding for myc-tagged wildtype NUP93 or the R537W and F699L variant. 0.15–0.2 μg/μl mRNA was added to achieve approximate endogenous NUP93 expression levels. The NUP93 antibody recognizes a slightly slower migrating cross-reactivity by Western blotting (*) which is neither immunoprecipitated nor depleted. **b** Nuclei assembled for 120 min in extracts generated (**a**) were analyzed by for formation of a closed nuclear envelope by membrane staining with DiIC18 (upper row, red) or immunofluorescence for NUP93 (green, second row); mAB414 (red, third row); MYC-tag (green, fifth row); or NUP58 (red, sixth row). DNA was stained with DAPI (blue). (Scale bar 10 μm). **c** Quantitation of chromatin substrates with a closed nuclear envelope. Columns represent the average of three independent experiments. Individual data points each from more than 100 randomly chosen chromatin substrates are indicated

Consistent with their important function, mutations in NPC components can cause human disorders [40]. Here, we identify patients with non-progressive congenital ataxia, associated with biallelic *NUP93* pathogenic variants. NUP93 is highly conserved in all eukaryotic phyla [41] and is essential for cellular nuclear transport (for review, see [7]). It is highly expressed in human brain and cerebellum (Supplemental Fig. S2B). It plays a crucial structural function in NPCs acting as an interaction hub within the inner ring ref. [8, 32, 42]. Consistently, NUP93 depletion blocks NPC assembly in *X. laevis* egg extracts [8, 37] and Fig. 4). We showed that the R537W variant cannot replace the wild type protein in NPC assembly acting as a functional null mutation, whereas the F699L variant localizes to NPCs and enables NPC assembly when replacing wild type NUP93 in in vitro nuclear assembly assays. Indeed, if both proteins were present in the in vitro assembly reaction, only the F699L variant localizes to NPCs (Supplemental Fig. S3). Given the crucial function of NUP93 conserved during evolution and the failure of R537W variant to allow NPC assembly, it is likely that the F699L variant ensures NPC function and hence survival in patient cells, since two loss-of-function *NUP93* mutations would be embryonic lethal and have therefore never been observed in human patients [16]. Interestingly, we have observed a similar pattern when analyzing *NUP93* variants in steroid-resistant nephrotic syndrome (SRNS). In those patients, one allele behaves as a functional null similarly to the R537W variant whereas the second one supported NPCs assembly. The homozygous, compound heterozygous missense or truncating variants of *NUP93* detected in SRNS families where a combination of a loss of function variant with a hypomorphic variant not affecting nuclear envelope integrity or NPC assembly [15]. In the in vitro nuclear assembly assay, combinations of two non-functional variants (R537W, identified in this work, and R388W found in SNRS patients [15]) did not allow for NPC assembly (Supplemental Fig. S3). In contrast, NPCs assembled whenever wild type NUP93 or the functional F699L or G591V variants, identified in this work or linked to SNRS [15], respectively (see also Fig. 2), were present. This indicates that neither R537W nor R388W act as dominant negatives consistent with their recessive inheritance pattern.

The NUP93 variants described here do not abrogate the interaction with NUP205 or NUP188 similarly to the NUP93 mutations linked to SNRS. Interestingly, the position F699 in NUP93 is surrounded by several conserved serines that are predicted to undergo phosphorylation. Nucleoporin phosphorylation have important functions in regulating protein-protein interactions in this network: NUP98 and NUP53 are phosphorylated at the onset of mitosis, which is important for breaking up nucleoporins interactions and induces NPC disassembly [38, 39]. Thus, it is tempting to speculate that the F699L change could impact NUP93 interactions to other nucleoporins or shuttling proteins in a cell cycle-dependent manner.

Monogenic mutations in genes encoding other NPC components have been described in other human diseases: pathogenetic variants in *NUP93*, *NUP205*, *NUP107*, *NUP85*, *NUP133*, and *NUP160* have been reported in SNRS as discussed above. *NUP107* and *NUP133* have been associated to nephrotic syndrome with microcephaly and cortical dysgenesis [16, 19, 20] whereas *NUP37* and *NUP62* have been associated with congenital microcephaly, intellectual disability, or bilateral striatal necrosis, respectively, without renal involvement [16, 21]. The nucleoporin ALADIN is mutated in syndromic cerebellar ataxia with neuropathy and adrenal insufficiency; compound heterozygous loss of function and hypomorphic variants have been reported in this syndrome [22, 43]. Despite the universal and essential function of NPCs in all nucleated cells, biallelic mutations in nucleoporins seem to have specific consequences causing distinct cellular and organ phenotypes. In the case of NUP93, the different mutations cause distinct cerebellar or renal disease phenotype. As the age of onset of SNRS is variable ranging from 0 to 3 months to adult age, we cannot exclude that the patients will later develop a renal disease although their urine analysis have been repeatedly normal. It will be an interesting and challenging research path to define how these different mutations in the same essential nucleoporin affect the different organs leading to diverse pathologies.

Acknowledgements The authors thank the patients and their family for their participation in this study.

Authors' Contribution Conceived and designed the project: GZ and WA. Performed the experiments: PDM, MN, EB, SB, AS, AC, MM, HL, and DMA. Analyzed the data: GZ, WA, EB, and MT. Contributed to the writing of the manuscript: GZ and WA. All authors approved the final version of this manuscript.

Funding This work was supported by grants from the Italian Ministry of Health (Ricerca Finalizzata NET-2013-02356160 to E.B), Fondazione

Bambino Gesù (Vite Coraggiose to M.T), and the German Research Foundation to W.A (AN377/7-1).

Compliance with Ethical Standards

All studies were performed in accordance with the Declaration of Helsinki. Written informed consent was obtained from all participating subjects.

Conflict of Interest The authors declare that they have no competing interests.

Publisher's Note Springer Nature remains neutral with regard to jurisdictional claims in published maps and institutional affiliations.

References

1. Steinlin M. Nonprogressive congenital ataxias. Brain Dev. 1998;4:199–208.
2. Bertini E, Zanni G, Boltshauser E. Nonprogressive congenital ataxias. Handb Clin Neurol. 2018;155:91–103.
3. Zanni G, Bertini E. X-linked ataxias. Handb Clin Neurol. 2018;155:175–89.
4. Wente SR, Rout MP. The nuclear pore complex and nuclear transport. Cold Spring Harb Perspect Biol. 2010;2:a000562.
5. Beck M, Hurt E. The nuclear pore complex: understanding its function through structural insight. Nat Rev Mol Cell Biol. 2017;18:73–89.
6. Hezwani M, Fahrenkrog B. The functional versatility of the nuclear pore complex proteins. Semin Cell Dev Biol. 2017;68:2–9.
7. Vollmer B, Antonin W. The diverse roles of the Nup93/Nic96 complex proteins—structural scaffolds of the nuclear pore complex with additional cellular functions. Biol Chem. 2014;395:515–28.
8. Sachdev R, Sieverding C, Flotenmeyer M, Antonin W. The C-terminal domain of Nup93 is essential for assembly of the structural backbone of nuclear pore complexes. Mol Biol Cell. 2012;23:740–9.
9. Chug H, Trakhanov S, Hulsmann BB, Pleiner T, Gorlich D. Crystal structure of the metazoan Nup62*Nup58*Nup54 nucleoporin complex. Science. 2015;350:106–10.
10. von Appen A, Kosinski J, Sparks L, Ori A, Di Guilio AL, Vollmer B, et al. In situ structural analysis of the human nuclear pore complex. Nature. 2015;526:140–3.
11. Vollmer B, Schooley A, Sachdev R, Eisenhardt N, Schneider AM, Sieverding C, et al. Dimerization and direct membrane interaction of Nup53 contribute to nuclear pore complex assembly. EMBO J. 2012;31:4072–84.
12. Mansfeld J, Guttinger S, Hawryluk-Gara LA, Pante N, Mall M, Galy V, et al. The conserved transmembrane nucleoporin NDC1 is required for nuclear pore complex assembly in vertebrate cells. Mol Cell. 2006;22:93–103.
13. De Magistris P, Tatarek-Nossol M, Dewor M, Antonin W. A self-inhibitory interaction within Nup155 and membrane binding are required for nuclear pore complex formation. J Cell Sci. 2018;131(1). https://doi.org/10.1242/jcs.208538.
14. Mitchell JM, Mansfeld J, Capitanio J, Kutay U, Wozniak RW. Pom121 links two essential subcomplexes of the nuclear pore complex core to the membrane. J Cell Biol. 2010;191:505–21.
15. Braun DA, Sadowski CE, Kohl S, Lovric S, Astrinidis SA, Pabst WL, et al. Mutations in nuclear pore genes NUP93, NUP205 and XPO5 cause steroid-resistant nephrotic syndrome. Nat Genet. 2016;48:457–65.
16. Braun DA, Lovric S, Schapiro D, Schneider R, Marquez J, Asif M, et al. Mutations in multiple components of the nuclear pore complex cause nephrotic syndrome. J Clin Invest. 2018;128(10):4313–28. https://doi.org/10.1172/JCI98688.
17. Miyake N, Tsukaguchi H, Koshimizu E, Shono A, Matsunaga S, Shiina M, et al. Biallelic mutations in nuclear pore complex subunit NUP107 cause early-childhood-onset steroid-resistant nephrotic syndrome. Am J Hum Genet. 2015;97:555–66.
18. Park E, Ahn YH, Kang HG, Miyake N, Tsukaguchi H, Cheong HI. NUP107 mutations in children with steroid-resistant nephrotic syndrome. Nephrol Dial Transplant. 2017;32:1013–7.
19. Rosti RO, Sotak BN, Bielas SL, Bhat G, Silhavy JL, Aslanger AD, et al. Homozygous mutation in NUP107 leads to microcephaly with steroid-resistant nephrotic condition similar to Galloway-Mowat syndrome. J Med Genet. 2017;54:399–403.
20. Fujita A, Tsukaguchi H, Koshimizu E, Nakazato H, Itoh K, Kuraoka S, et al. Homozygous splicing mutation in NUP133 causes Galloway-Mowat syndrome. Ann Neurol. 2018;84:814–28. https://doi.org/10.1002/ana.25370.
21. Basel-Vanagaite L, Muncher L, Straussberg R, Pasmanik-Chor M, Yahav M, Rainshtein L, et al. Mutated nup62 causes autosomal recessive infantile bilateral striatal necrosis. Ann Neurol. 2006;60:214–22.
22. Tullio-Pelet A, Salomon R, Hadj-Rabia S, Mugnier C, de Laet MH, Chaouachi B, et al. Mutant WD-repeat protein in triple-a syndrome. Nat Genet. 2000;26:332–5.
23. Kortüm F, Caputo V, Bauer CK, Stella L, Ciolfi A, Alawi M, et al. Mutations in KCNH1 and ATP6V1B2 cause Zimmermann-Laband syndrome. Nat Genet. 2015;47:661–7.
24. McKenna A, Hanna M, Banks E, Sivachenko A, Cibulskis K, Kernytsky A, et al. The genome analysis toolkit: a MapReduce framework for analyzing next-generation DNA sequencing data. Genome Res. 2010;9:1297–303.
25. Sferra A, Baillat G, Rizza T, Barresi S, Flex E, Tasca G, et al. TBCE mutations cause early-onset progressive encephalopathy with distal spinal muscular atrophy. Am J Hum Genet. 2016;99:974–83.
26. Li H, Durbin R. Fast and accurate short read alignment with burrows-wheeler transform. Bioinformatics. 2009;25:1754–60.
27. Cingolani P, Platts A, le Wang L, Coon M, Nguyen T, Wang L, et al. A program for annotating and predicting the effects of single nucleotide polymorphisms, SnpEff: SNPs in the genome of Drosophila melanogaster strain w1118; iso-2; iso-3. Fly. 2012;6:80–92.
28. Liu X, Jian X, Boerwinkle E. dbNSFP v2.0: a database of human non-synonymous SNVs and their functional predictions and annotations. Hum Mutat. 2013;34:E2393–402.
29. Kircher M, Witten DM, Jain P, O'Roak BJ, Cooper GM, Shendure J. A general framework for estimating the relative pathogenicity of human genetic variants. Nat Genet. 2014;46:310–5.
30. Dong C, Wei P, Jian X, Gibbs R, Boerwinkle E, Wang K, et al. Comparison and integration of deleteriousness prediction methods for nonsynonymous SNVs in whole exome sequencing studies. Hum Mol Genet. 2015;24:2125–37.
31. Eisenhardt N, Schooley A, Antonin W. Xenopus in vitro assays to analyze the function of transmembrane nucleoporins and targeting of inner nuclear membrane proteins. Methods Cell Biol. 2014;122:193–218.
32. Theerthagiri G, Eisenhardt N, Schwarz H, Antonin W. The nucleoporin Nup188 controls passage of membrane proteins across the nuclear pore complex. J Cell Biol. 2010;189:1129–42.
33. Morlan J, Baker J, Sinicropi D. Mutation detection by real-time PCR: a simple, robust and highly selective method. PLoS One. 2009;4:e4584.
34. Kosinski J, Mosalaganti S, von Appen A, Teimer R, Di Guilio AL, Wan W, et al. Molecular architecture of the inner ring scaffold of the human nuclear pore complex. Science. 2016;352:363–5.

35. Nagata K, Randall A, Baldi P. SIDEpro: a novel machine learning approach for the fast and accurate prediction of side-chain conformations. Proteins. 2012;80:142–53.
36. Gant TM, Wilson KL. Nuclear assembly. Annu Rev Cell Dev Biol. 1997;13:669–95.
37. Grandi P, Dang T, Pane N, Shevchenko A, Mann M, Forbes D, et al. Nup93, a vertebrate homologue of yeast Nic96p, forms a complex with a novel 205-kDa protein and is required for correct nuclear pore assembly. Mol Biol Cell. 1997;8:2017–38.
38. Laurell E, Beck K, Krupina K, Theerthagiri G, Bodenmiller B, Horvath P, et al. Phosphorylation of Nup98 by multiple kinases is crucial for NPC disassembly during mitotic entry. Cell. 2011;144:539–50.
39. Linder MI, Kohler M, Boersema P, Weberruss M, Wandke C, Marino J, et al. Mitotic disassembly of nuclear pore complexes involves CDK1- and PLK1-mediated phosphorylation of key interconnecting nucleoporins. Dev Cell. 2017;43:141–156.e147.
40. Nofrini V, Di Giacomo D, Mecucci C. Nucleoporin genes in human diseases. Eur J Hum Genet. 2016;24:1388–95.
41. Neumann N, Lundin D, Poole AM. Comparative genomic evidence for a complete nuclear pore complex in the last eukaryotic common ancestor. PLoS One. 2010;5:e13241.
42. Stuwe T, Bley CJ, Thierbach K, Petrovic S, Schilbach S, Mayo DJ, et al. Architecture of the fungal nuclear pore inner ring complex. Science. 2015;350:56–64.
43. Koehler K, Brockmann K, Krumbholz M, Kind B, Bönnemann C, Gärtner J, et al. Axonal neuropathy with unusual pattern of amyotrophy and alacrima associated with a novel AAAS mutation p.Leu430Phe. Eur J Hum Genet. 2008;16:1499–506.